Supporting information for

Au@Ag Nanoparticles: Halides Stabilize {100} Facets

Sergio Gómez-Graña,[a] Bart Goris,[b] Thomas Altantzis,[b] Cristina Fernández-López,[a] Enrique Carbó-Argibay,[a] Andres Guerrero-Martínez,[a,c] Neyvis Almora-Barrios,[d] Nuria López,[d] Isabel Pastoriza-Santos,[a] Jorge Pérez-Juste,[a] Sara Bals,[b] Gustaaf Van Tendeloo,[b] and Luis M. Liz-Marzán[a,e,f]

[a] *Departamento de Química Física, Universidade de Vigo, 36310 Vigo, Spain.*

[b] *EMAT-University of Antwerp, Groenenborgerlaan 171, B-2020 Antwerp, Belgium.*

[c] *Department of Physical Chemistry I, Complutense University of Madrid Avda. Complutense s/n, 28040 Madrid, Spain*

[d] *Institute of Chemical Research of Catalonia, ICIQ, Av. Països Catalans, 16, 43007 Tarragona, Spain*

[e] *BioNanoPlasmonics Laboratory, CIC biomaGUNE, Paseo de Miramón 182, 20009 Donostia - San Sebastián, Spain*

[f] *Ikerbasque, Basque Foundation for Science, 48011 Bilbao, Spain*

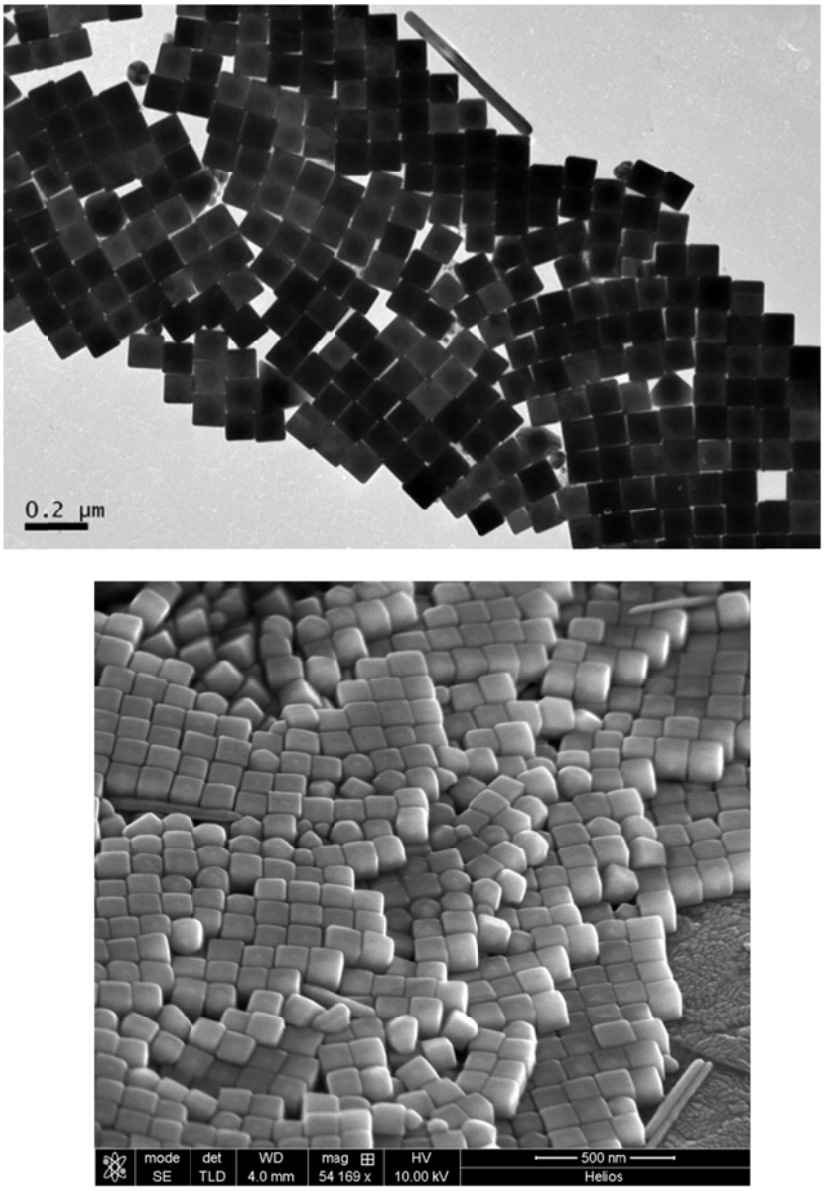

Figure S1. Representative TEM (upper row) and SEM (lower row) images of the Au@Ag cubes.

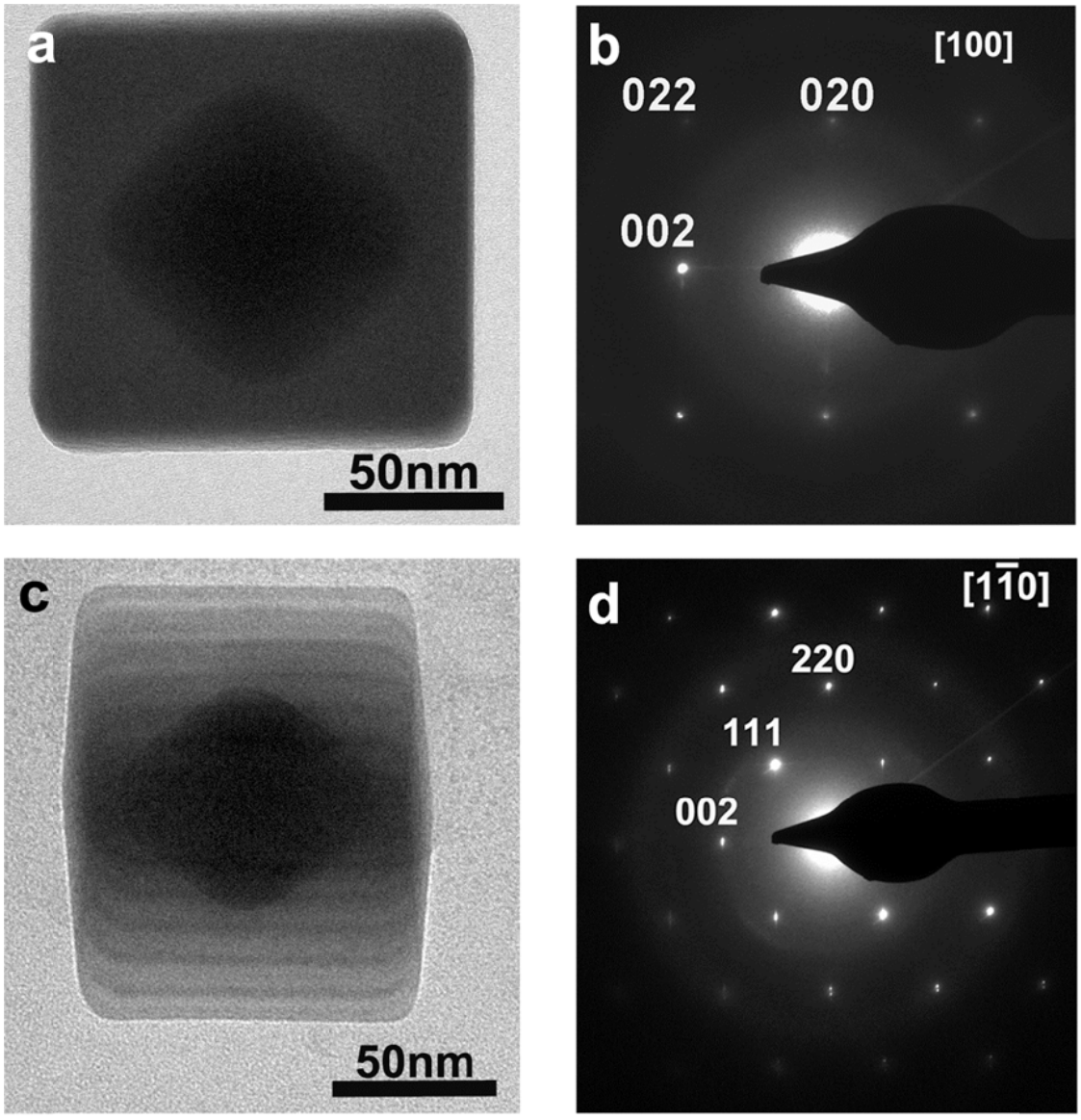

Figure S2. (a) TEM image of the same particle lying on an edge parallel to the [001] direction and (c) after being rotated 45º along the [001]. Therefore the observed parallel fringes of equal-thickness observed in the top and bottom sides of the cube are a consequence of that orientation. (b and d) acquired selected area diffraction patterns of the projections in figures a and c respectively.

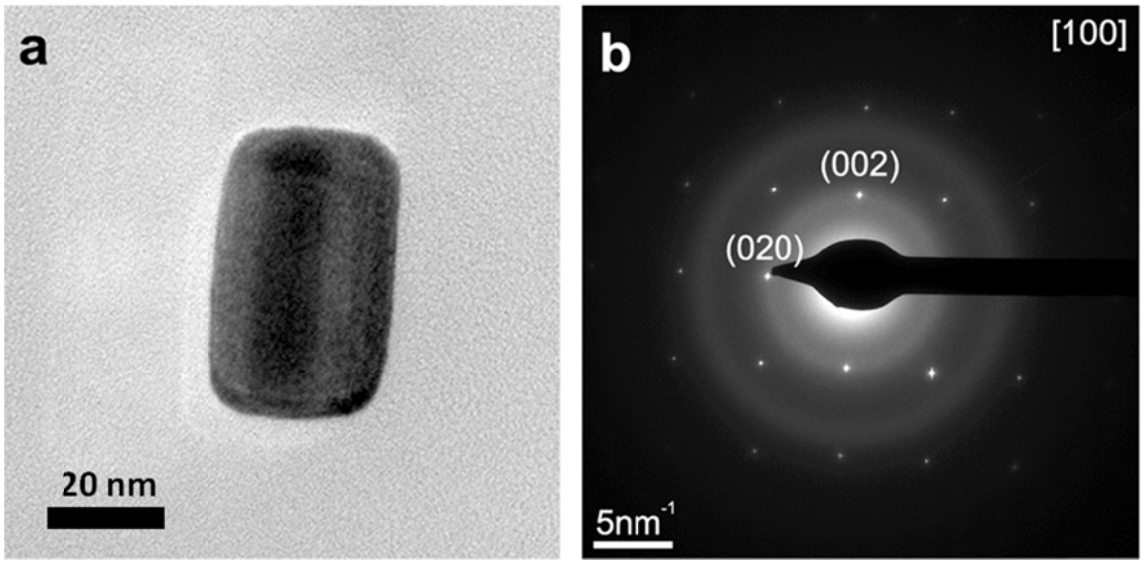

Figure S3. (a) TEM projection and (b) acquired selected area diffraction pattern of an Au@AgNR on a carbon support. The diffraction pattern indicates that the nanorod is viewed along a [100] zone axis. The absence of splitting indicates the epitaxial growth of Ag on the Au rod.

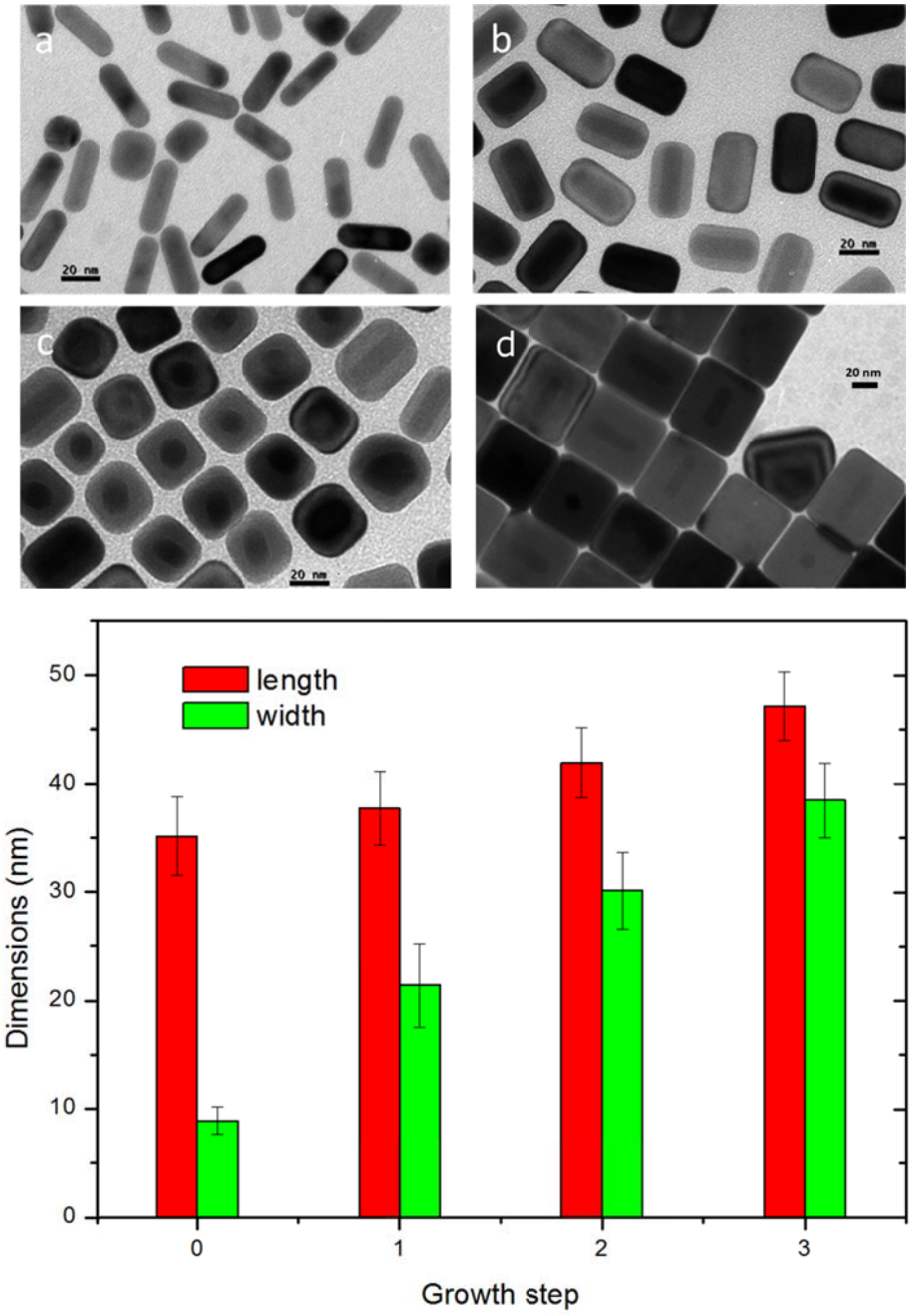

Figure S4. Representative TEM images of the initial AuNRs (a) and after one (b), two (c) and three (d) growth steps. Average dimensions of the initial AuNRs and after each growth step.

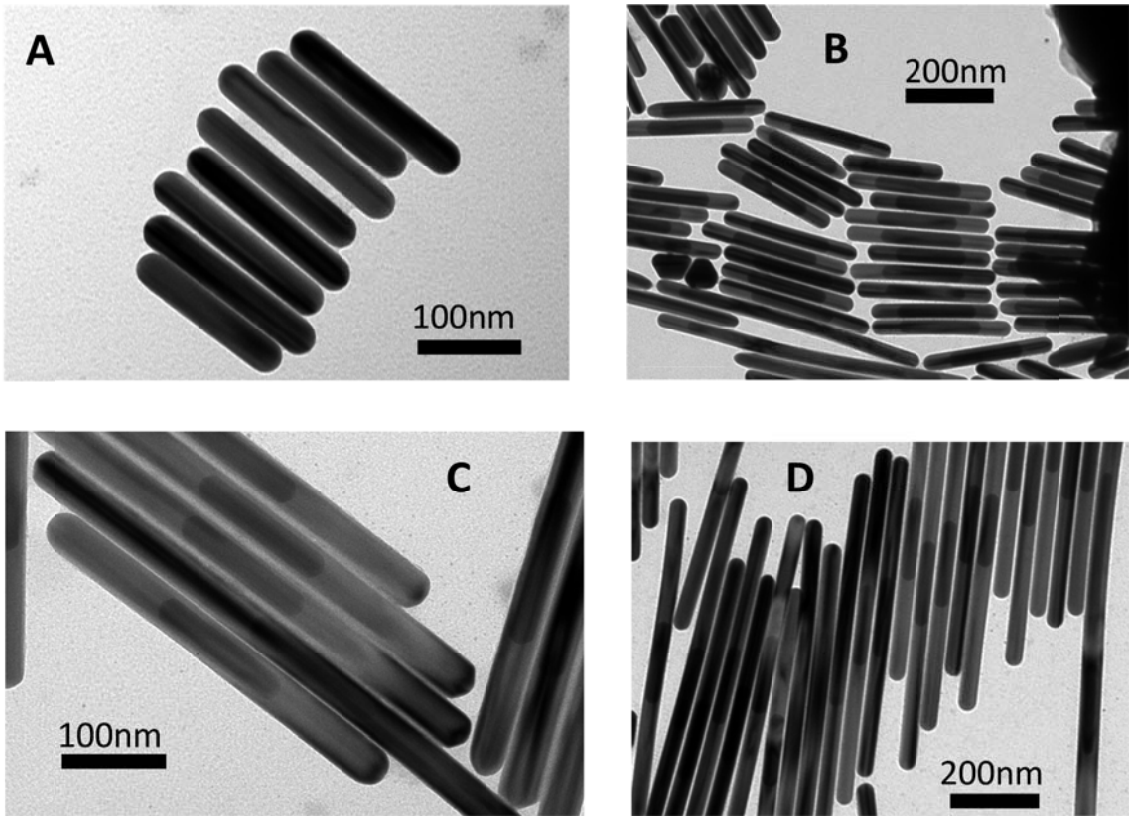

Figure S5. Representative TEM images of the initial pentatwinned AuNRs (A) and after three different growth steps. It can be observed that the average length of the Au@AgNR increases from B to D while the width remains almost constant.

Table S1. Surface energies, γ in J/m^2, for the lowest-index surfaces of relevant structures. The surface energy was calculated as follows:

$$\gamma_X = \frac{(E_{non-relaxed\ slab} - N\,E_{bulk})}{2A} + \frac{(E_{relaxed\ slab} - E_{non-relaxed\ slab})}{A}$$

where X represents the surface and A its corresponding area; $E_{non\text{-}relaxed\text{-}slab}$ is the energy for the as cut slab $E_{relaxed\text{-}slab}$ is the slab energy upon relaxation.

	(111)	(100)	(110)
Au	0.736	0.882	0.917
Au@Ag(2ML)	0.939	0.946	0.948

Table S2. Adsorption energies, E_{ads} in eV, and their contribution to the surface energy γ'=γ+ΔE/A in J/m^2, for the lowest-index surfaces of relevant structures. Adsorption energies were calculated with respect to gas-phase X_2 or the crystal halide AgX. For AgX, E_{ads}=ΔE. Instead, for the halide, X^-, $\Delta E = E_{solv} + EA - \phi + E_{ads}$, as it includes the solvation energy of the halide, E_{solv}, its electron affinity, *EA*, the work function of the metal, ϕ, and the adsorption energy of the neutral halogen atom X.

	E_{ads}(111)	γ' (111)	E_{ads}(100)	γ'(100)	E_{ads}(110)	γ'(110)
Cl	-1.01	1.074	-1.66	0.462	-1.56	0.668
Br	-0.82	0.864	-1.57	0.204	-1.56	0.426
AgCl	--	0.939	-0.61	0.603	-0.86	0.635
AgBr	--	0.939	-0.90	0.468	-0.95	0.479